Your thesaurus codes are:
12(02.16.2; 09.19.1; 10.07.1; 12.03.1; 13.18.3)

ASTROPHYSICS
September 12, 2000

Power spectrum of the polarized diffuse Galactic radio emission

C. Baccigalupi[1], C. Burigana[2], F. Perrotta[1], G. De Zotti[3], L. La Porta[2], D. Maino[4], M. Maris[4], and R. Paladini[1]

[1] SISSA/ISAS, Via Beirut 4, I-34014 Trieste, Italy
[2] ITeSRE/CNR, Via P. Gobetti 101, I-40129 Bologna, Italy,
[3] Osservatorio Astronomico di Padova, Vicolo dell'Osservatorio 5, I-35122 Padova, Italy
[4] Osservatorio Astronomico di Trieste, Via Tiepolo 11, I-34131 Trieste, Italy

the date of receipt and acceptance should be inserted later

Received / Accepted

Abstract. We have analyzed the available polarization surveys of the Galactic emission to estimate to what extent it may be a serious hindrance to forthcoming experiments aimed at detecting the polarized component of Cosmic Microwave Background (CMB) anisotropies. Regions were identified for which independent data consistently indicate that depolarization must be small. The power spectrum of the polarized emission, in terms of antenna temperature, was found to be described by $C_\ell \simeq (1.2 \pm 0.8) \cdot 10^{-9} \cdot (\ell/450)^{-1.8\pm0.3} \cdot (\nu/2.4\mathrm{GHz})^{-5.8}$ K^2, from arcminute to degree scales. Data on larger angular scales ($\ell \leq 100$) indicate a steeper slope $\sim \ell^{-3}$. We conclude that polarized Galactic emission is unlikely to be a serious limitation to CMB polarization measurements at the highest frequencies of the MAP and Planck/LFI instruments, at least for $\ell \geq 50$ and standard cosmological models. The weak correlation between polarization and total power and the low polarization degree of radio emission close to the Galactic plane, found also in low-depolarization regions, is interpreted as due to large contributions to the observed intensity from unpolarized sources, primarily strong HII regions, concentrated on the Galactic plane. Thus estimates of the power spectrum of total intensity at low Galactic latitudes are not representative of the spatial distribution of Galactic emission far from the plane. Both total power and polarized emissions show highly significant deviations from a Gaussian distribution.

Key words: Polarization – ISM: structure – Galaxy: general – cosmology: cosmic microwave background – radio continuum: ISM

1. Introduction

Several ongoing or planned experiments (see Staggs et al. 1999 for a recent review) are designed to reach the sensitivities required to measure the expected linear polarization of the Cosmic Microwave Background (CMB).

The forthcoming space missions Planck and MAP, aimed at obtaining full sky high sensitivity and high resolution maps of CMB anisotropies will also probe the CMB polarization fluctuations (Mandolesi et al. 1998; Puget et al. 1998; and the MAP webpage: `http://map.gsfc.nasa.gov/`).

The current design of instruments for the Planck mission (the third Medium-size mission of ESA's Horizon 2000 Scientific Programme) provides good sensitivity to polarization at all LFI (Low Frequency Instrument) frequencies (30, 44, 70, and 100 GHz) as well as at three HFI (High Frequency Instrument) frequencies (143, 217 and 545 GHz). The NASA's MIDEX class mission MAP has also polarization sensitivity in all channels (22, 33, 40, 61 and 98 GHz).

While there is a very strong scientific case for CMB polarization measurements (cf., e.g., Zaldarriaga 1998 and references therein), they are very challenging both because of the weakness of the signal and because of the contamination by foregrounds that may be more polarized than the CMB.

Our knowledge of polarized foreground components is very meager (see Davies & Wilkinson 1999 for a recent review). In this paper we present a preliminary investigation of the power spectrum of the polarized Galactic synchrotron emission, the likely dominant foreground contribution at microwave frequencies, at least at intermediate to large angular scales. When this work was approaching completion we learned that a similar analysis was carried out by Tucci et al. (2000). We improve on their results by taking into account, in addition to the Parkes survey (Duncan et al. 1995, 1997; hereafter D97) discussed by them, the more recent Effelsberg surveys at 2.7 GHz (Duncan et al. 1999; D99) and at 1.4 GHz, covering areas up to $\pm 20°$ of Galactic latitude (Uyaniker et al. 1998, 1999; U99), as well as the Leiden surveys (Brouw & Spoelstra 1976; BS76). We also discuss in some detail the effect of

the emission from HII regions in the Galactic plane and of the Faraday depolarization.

The Galactic polarized thermal dust emission, prevailing at frequencies beyond the CMB peak has been modelled by Prunet et al. (1998). De Zotti et al. (1999) discussed polarization fluctuations due to extragalactic sources. Additional polarized contributions are expected from magneto-dipole emission or rotational emission of dust grains (Draine & Lazarian 1999; Lazarian & Draine 2000) and scattered free-free emission (Keating et al. 1998). A multifrequency Wiener filtering method to detect CMB polarization in the presence of polarized foregrounds has been worked out by Bouchet et al. (1999).

2. Polarization surveys

Linear polarization observations extending up to high Galactic latitudes and carried out at several frequencies, from 408 to 1411 MHz, have been presented by BS76 (Leiden surveys). The half power beamwidths varied with increasing frequency from 2.3° to 0.6°. Unfortunately these and the other surveys discussed by Spoelstra (1984) are undersampled so that proper smoothing to the largest beamwidth, as required to combine data at different frequencies, is not possible. Thus, estimates of differential polarization and differential Faraday rotation across the beam cannot be made. The exact sky coverage and the number of available directions with the Stokes parameters Q and U measures (~ 2000) and their direction dependent sensitivity are different for the five frequency channel, with some patches in the sky better sampled then the average.

High resolution polarimetric surveys of strips around the Galactic plane at 2.4 and 2.695 GHz, respectively, have recently presented by D97 and D99. U99 carried out a surface brightness and polarization survey of four fields at medium Galactic latitudes (up to $b = 20°$), at 1.4 GHz. These data, together with details about the instrumental capabilities, can be found at the WEB site HTTP://WWW.MPIFR-BONN.MPG.DE/SURVEY.HTML.

D97 covered 127° of Galactic longitude ($238° < l < 5°$) out to at least $b = \pm 5°$ (for $340° < l < 5°$ the survey extends to $b = +7°$, for $340° < l < 352°$ to $b = -7°$, and for $240° < l < 270°$ to $b = -8°$) with an angular resolution of 10.4′. The surveyed area amounts to $\simeq$ 1413 square degrees. The nominal rms noise for total power is of 17 mJy/beam area (8 mK), and 11 mJy/beam area (5.3 mK) for polarization; however a lower rms noise of 11 mJy/beam area (5.3 mK) for total intensity and 6 mJy/beam area (2.9 mK) for polarization has been achieved over $\simeq$ 43% of the total area. The center frequency is 2.417 GHz and the bandwidth of about 145 MHz. Values of the Stokes Q and U parameters and of the total power are given for $4' \times 4'$ pixels, in units of mJy/beam area; the conversion factor to brightness temperature is 1 mJy/beam area = 0.48 mK (Duncan, private communication).

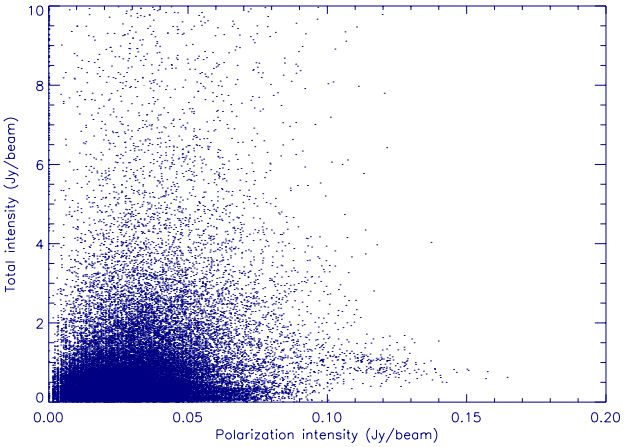

Fig. 1. Total versus polarized intensity in the $300° \leq l \leq 320°$ region from the D97 data at 2.4 GHz, showing no correlation at all.

Polarimetric data from the Effelsberg 2.695 GHz survey with half-power beamwidth of 4.3′ in the first Galactic quadrant were reported by D99. Maps at a resolution of 5.1′ of the Stokes Q and U emission components, covering the region $74° \geq l \geq 4°.9$, $|b| \leq 5°$, with a rms noise of 2.5 mJy/beam area (corresponding to 9 mK) were constructed.

Of particular interest for our purposes is the continuum and polarization survey, also carried out with the Effelsberg 100-m telescope, at medium Galactic latitudes (up to $b = \pm 20°$). Four areas were observed, totaling about 1050 sq. deg.: one in the first Galactic quadrant ($45° \geq l \geq 55°$, $4° \geq b \geq 20°$); the northern ($65° \geq l \geq 95°$, $5° \geq b \geq 15°$) and the southern ($70° \geq l \geq 100°$, $-15° \geq b \geq -5°$) parts of the Cygnus region; the highly polarized "fan region" ($140° \geq l \geq 153°$, $3.5° \geq b \geq 10°$); the anticentre region ($190° \geq l \geq 210°$, $3.8° \geq b \geq 15°$). The rms noise is about 15 mK (about 7 mJy/beam area) for total intensity and about 8 mK in linear polarization; the angular resolution is 9.35′.

3. Depolarization

A comparison of total power and polarized emission maps (Duncan et al. 1995, 1997; Uyaniker et al. 1998, 1999) shows little correlation. While the total intensity clearly peaks on the Galactic Plane (apart from a number of spurs and loops extending to high Galactic latitude), the polarized intensity is much more uniformly distributed. Also, many sources which are very intense in total power are not seen in polarized emission and, conversely, bright regions of extended polarization do not appear to be connected with sources of total-power emission (D97, U99).

This is can be seen in Fig.1, showing, as an example, the polarization intensity $\sqrt{Q^2 + U^2}$ versus the to-

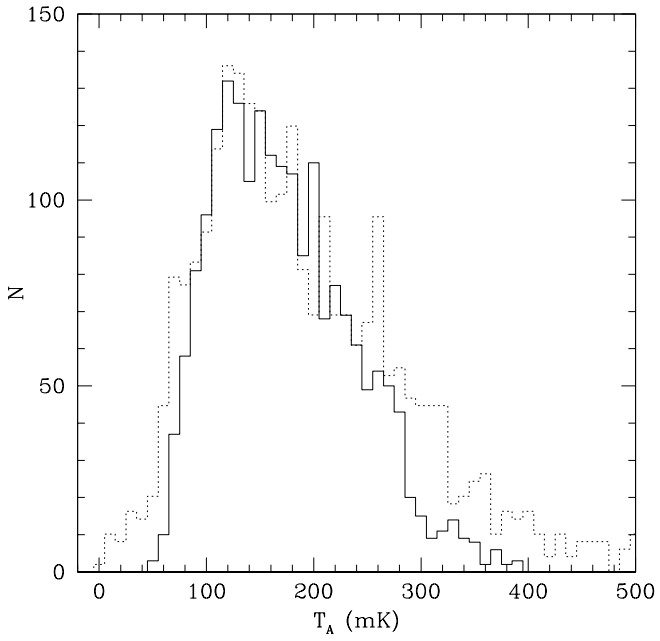

Fig. 2. Comparison of distributions of polarized (solid line) and total intensities (dot-dashed line) for the U99 region centered at $l = 146^\circ.4$. To ease the comparison, the polarization distribution has been shifted by 60 mK along the x-axis and the amplitude of the total intensity distribution has been increased by a factor of 1.3 in order to roughly superpose the two peaks. See also the caption to Fig. 3.

tal intensity for the Parkes survey data in the region $300^\circ \leq l \leq 320^\circ$ and $|b| \leq 5^\circ$.

Two main factors may contribute to this situation. On one side, many bright structures on the Galactic plane are (unpolarized) HII regions and significant thermal radio emission is also expected between and above bright HII regions in our Galaxy: Duncan et al. (1995) estimate a thermal flux level of the order of 100 mJy per beam area at 2.4 GHz, comparable to the level of the radio continuum often observed near these regions. The large thermal contributions to the Galactic emission, which are concentrated close to the Galactic plane, obviously make very unlikely that the total intensity power spectra for these regions can be representative of the power spectra at high Galactic latitudes.

On the other side, differential Faraday rotation or variations of the magnetic field orientation may strongly depolarize the emission from distant regions of the Galaxy (Burn 1966, Gardner & Whiteoak 1966) so that only the polarized emission of relatively local origin can be observed. The two factors may act together: variations in the density of thermally emitting electrons may lead to a large enough differential Faraday rotation to produce substantial depolarization; in addition, the magnetic field may be tangled by turbulent motions of the ionized gas, leading to further depolarization.

The Faraday rotation of the polarization position angle of a linearly polarized wave at a wavelength λ traversing an ionized medium with electron density n_e and magnetic field $\mathbf{B}$ is given by:

$$\phi(\lambda) = \mathrm{RM}\lambda^2 \ \mathrm{rad}, \tag{1}$$

where the rotation measure RM is the line-of-sight integral

$$\begin{aligned} \mathrm{RM} &= \frac{e^3}{2\pi m_e^2 c^4} \int n_e \mathbf{B} \cdot d\mathbf{l} = \\ &= 810 \int n_e(\mathrm{cm}^{-3}) B_\parallel(\mu\mathrm{G}) \cdot dl(\mathrm{kpc}) \ \mathrm{rad\,m}^{-2}. \end{aligned} \tag{2}$$

Since ϕ scales as ν^{-2}, the Faraday rotation is likely irrelevant at microwaves, where MAP and Planck instruments will operate, while it may strongly distort the power spectrum of polarized emission at the decimetric wavelengths considered here, on one side by wiping out polarized emission from far regions (due to differential rotation within the beamwidth or the bandwidth of observations) and, on the other side, introducing structure on a variety of scales (larger than the beamwidth) due to fluctuations in the thermal electron density distribution and/or magnetic field variations (in strength and/or direction) along the line of sight.

If the synchrotron emission arises throughout the depth of the Faraday rotating medium, the polarization is reduced from the intrinsic value P_0 to (Burn 1966):

$$P(\lambda) = P_0 \frac{\sin\phi}{\phi} \ . \tag{3}$$

For $\phi = 1\,\mathrm{rad}$, corresponding to $\mathrm{RM}(\mathrm{rad\,m}^{-2}) = 21.8$, 64.1, and 80.8 for $\nu = 1.4$, 2.4, and 2.7 GHz, respectively, the depolarization amounts to about 16%. Spoelstra (1984), from his analysis of multifrequency data on linear polarization, found that the distribution of RM over the sky shows a complex pattern with typical values (in the region covered by Leiden surveys) of $8\,\mathrm{rad\,m}^{-2}$.

The Galactic RM distribution is also probed by Faraday rotation measurements towards pulsars and extragalactic radio sources. Since pulsar distances can often be independently derived, pulsar data also provide information on the variation of RM along the line of sight; also, their appear to have no intrinsic Faraday rotation and hence their observed RM arises entirely along the path to the observer. Extragalactic sources can provide information on the Galactic medium out to large distances, beyond those where pulsars are found; on the other hand, extragalactic sources may have their own Faraday rotation which adds to the Galactic contribution.

A catalogue of known pulsars, including values of RM, has been published by Taylor et al. (1993); an updated version is available via ftp (see Appendix of Taylor et al. 1993). Additional RMs have been published by Manchester & Johnston (1995), Navarro et al. (1997) and Han et al. (1999); on the whole, we have collected RMs for 318 pulsars.

Rotation measures for 674 extragalactic sources have been catalogued by Broten et al. (1988). Additional RMs have been published by Clegg et al. (1992).

An analysis of the RM of pulsars and extragalactic sources located in the sky areas covered by polarization surveys considered here reveals a number of regions where RMs can produce only a small Faraday depolarization ($\phi \leq 1\,\mathrm{rad}$). One of these is the area $140^\circ \leq l \leq 153^\circ$, $3^\circ.7 \leq b \leq 10^\circ$, surveyed by U99. This partly covers the highly polarized region referred to as the "fan region" where the rotation measures have long been known to be small (Bingham & Shakeshaft 1967) and the magnetic field direction has to be basically perpendicular to the line of sight.

The distribution of polarized intensities is closely similar to that of total intensities (Fig. 2): the main difference is the far more extended bright tail of total intensities, corresponding to low polarization sources. This strongly suggests that there is no significant depolarization in this region.

Due to the difficulty in obtaining a high accuracy absolute calibration of Galactic emission (the dominant contribution to the observed intensity comes from the Cosmic Microwave Background whose antenna temperature has a rms uncertainty of about 320 mK at 1.4 GHz (Staggs et al. 1996, Sironi et al. 1999), and a significant, though uncertain, contribution also comes from unresolved extragalactic sources (Toffolatti et al. 1989), the polarization degree cannot be reliably estimated. However, the data by U99 do indicate a high value, within a factor of less than two of the theoretical maximum corresponding to a uniform magnetic field (Ginzburg & Syrovatskii 1965):

$$\Pi = \frac{3-3\beta}{1-3\beta}\,, \tag{4}$$

for a typical value, $\beta = 2.9$, of the spectral index of the antenna temperature of synchrotron emission ($T_A \propto \nu^{-\beta}$; $\Pi(2.9) \simeq 75\%$). Again, this is suggestive of negligible depolarization, not only by Faraday rotation but also by magnetic field structure. The distribution of polarized intensities for the region centered at $l = 50^\circ$ (Fig. 4) is clearly narrower than for the "fan region" (Fig. 3) consistent with a considerable depletion of the high polarization tail.

The distributions for the anticenter region (centered at $l = 200^\circ$) is intermediate between the two regions above and consistent with moderate depolarization effects.

The region centered at $l = 80^\circ$ contains strong emission from local sources (U99), including three polarized supernova remnants and the radio galaxy Cygnus A. It also contains the large X-ray halo called the Cygnus superbubble. Thus it is certainly not a typical region. The distribution of polarized intensities is much broader than observed in any other region, reflecting its complex polarization structure, with steep gradients possibly due to spatially varying depolarization.

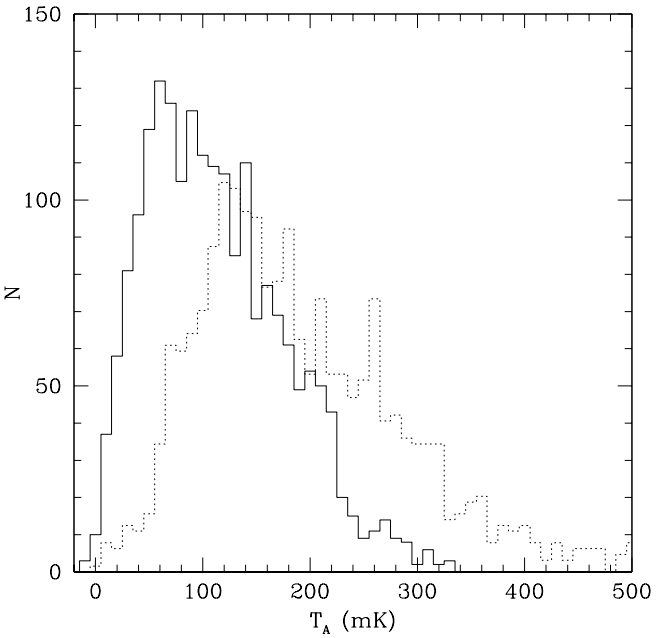

Fig. 3. Distributions of polarized (solid line) and total intensities (dot-dashed line) for the U99 region centered at $l = 146^\circ.4$. The total intensity antenna temperatures available at http://www.mpifr-bonn.mpg.de/staff/buyaniker/index.htm have a substantial negative tail coming out from the adopted procedure for subtracting the isotropic background (Uyaniker, private communication). To cure this, we have applied a constant correction $\Delta T_A = 112\,\mathrm{mK}$, making all values ≥ 0. Note that the total intensity and polarization maps available on the Web have somewhat different angular resolutions (about $5'$ and $4'$, respectively), which in both cases are smaller than the telescope beamwidth ($9.35'$). In order to have data on independent cells on the sky we have plotted the signals averaged over 3×3 pixels. Also the distributions are scaled to the same number of elements.

It is clear from Figs. 3 and 4 that the distributions of both total and polarized emissions are distinctly non-Gaussian. The statistical significance of this visual impression can quantified by computing the moments of order > 2:

$$\mu_{\mathrm{i}} = \frac{\sum_{j=1}^{n} (S_{\mathrm{j}} - \bar{S})^{\mathrm{i}}}{n-1}\,. \tag{5}$$

It is convenient to define the dimensionless quantities $\beta_1 = \mu_3^2/\mu_2^3$, $\beta_2 = \mu_4/\mu_2^4$, $\beta_3 = \mu_3\mu_5/\mu_2^4$, $\beta_4 = \mu_6/\mu_2^3$, $\beta_5 = \mu_7\mu_3/\mu_2^5$, $\beta_6 = \mu_8/\mu_2^4$.

Usual definitions of skewness and of kurtosis are skewn $= \sqrt{\beta_1}$ and kurt $= \beta_2 - 3$, which vanish for a Gaussian distribution. The probable errors of β_1 and β_2 are given by (Pearson 1924) $0.6745\Sigma_{\beta_1}$ and $0.6745\Sigma_{\beta_2}$, respectively, with

$$\Sigma_{\beta_1} = (\beta_1/n)^{1/2} \cdot \\ \cdot\ (4\beta_4 - 24\beta_2 + 36 + 9\beta_1\beta_2 - 12\beta_3 + 35\beta_1)^{1/2} \tag{6}$$

Table 1. Moments of the distributions of total and polarized intensities.

	mean (mK)		σ (mK)		skewness		kurtosis	
	int	pol	int	pol	int	pol	int	pol
Uyaniker $l = 50°$	319*	154	210	89	63 ± 26	1.32 ± 0.12	144 ± 35	3.15 ± 0.25
Uyaniker $l = 80°$	589*	92	718	1005	26.5 ± 2.0	1010 ± 235	35.4 ± 3.4	1010 ± 239
Uyaniker $l = 146°.4$	209*	112	160	64	22.0 ± 4.9	0.364 ± 0.036	38.6 ± 8.0	-0.089 ± 0.083
Uyaniker $l = 200°$	228*	70	145	40	50 ± 6	0.44 ± 0.08	78 ± 9.5	0.72 ± 0.51
D97 $240° \leq l \leq 260°$	161	13	110	9	55 ± 36	0.26 ± 0.02	211 ± 83	0.076 ± 0.068
no sources	129		70		0.0035 ± 0.0031		-0.145 ± 0.025	
D97 $280° \leq l \leq 300°$	425	106	1741	33	339 ± 43	0.98 ± 0.05	468 ± 59	1.04 ± 0.13
no sources	192		227		1.41 ± 0.04		0.53 ± 0.07	
D97 $300° \leq l \leq 320°$	577	15	930	15	94 ± 23	0.88 ± 0.05	196 ± 32	0.72 ± 0.16
no sources	423		404	0.59 ± 0.02		-0.22 ± 0.04		
D99 $20° \leq l \leq 30°$	317	32	907	20	131 ± 40	1.3 ± 0.3	269 ± 67	3.8 ± 1.9
D99 $55° \leq l \leq 65°$	72	32	18	11	1480 ± 337	0.49 ± 0.03	2440 ± 285	0.6 ± 0.1

* See text.

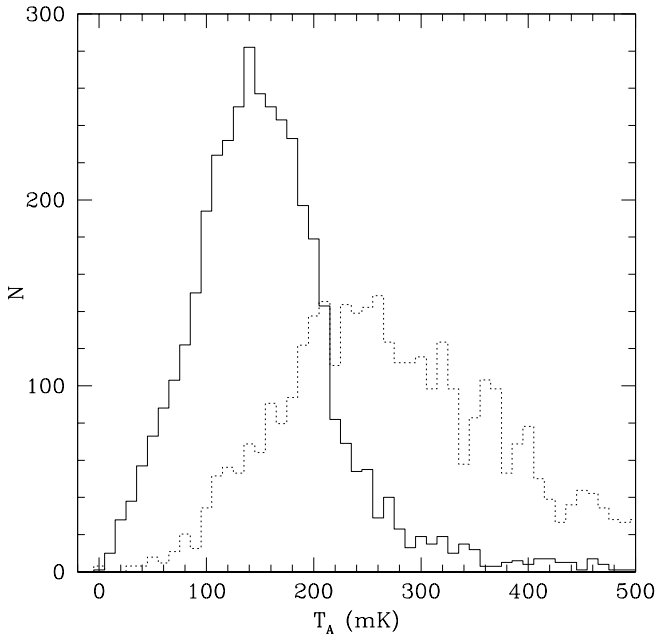

Fig. 4. Distributions of polarized (solid line) and total intensities (dot-dashed line) for the U99 region centered at $l = 50°$. In this case $\Delta T_A = 200\,\mathrm{mK}$ (see caption to Fig. 3).

$$\Sigma_{\beta_1} \; = \; n^{-1/2} \; .$$
$$\cdot(\beta_6 \; - \; 4\beta_2\beta_4 + 4\beta_2^3 - \beta_2^2 + 16\beta_1\beta_2 - 8\beta_3 + 16\beta_1)^{1/2} \quad (7)$$

The values of skewness and kurtosis for the regions we have analyzed, and their errors, are given in Table 1, together with the mean intensity and polarization degree and their standard deviations σ. It must be mentioned that the total intensity antenna temperatures given by U99 have a substantial negative tail coming out from the adopted procedure for subtracting the isotropic background (Uyaniker, private communication). To cure this, we have applied a constant offset to the values given for each region in order to making all values ≥ 0. The offsets are: $\Delta T_A = 200\,\mathrm{mK}$, 331 mK, 112 mK, and 157 mK, respectively, for the regions centered at $l = 50°$, 80°, 146°.4, and 200°.

The deviations from the Gaussian value (zero) of both skewness and kurtosis are in general highly significant, both for total and for polarized emissions. This may be a difficulty for methods involving Wiener filtering of the data to remove foreground contributions to CMB maps (Bouchet et al. 1999) since a Gaussian approximation for the distribution of foreground signals is assumed. On the other hand, Independent Component Analysis algorithms (Baccigalupi et al. 2000) require that all independent components contributing to the observed maps, except, at most, one have non-Gaussian distributions.

4. Intensity and polarization power spectra

The spherical harmonic expansion of the sky signal writes:

$$s(\hat{n}) = \sum_{\ell m} a_{\ell m} Y_\ell^m(\hat{n}) \; , \quad (8)$$

where $\hat{n}$ is the unit vector in the direction (θ, ϕ). The correlation function $C(\theta) =< s(\hat{n})s(\hat{n}') >_{\hat{n}\cdot\hat{n}'=\cos(\theta)}$ can be expanded into Legendre polynomials, with coefficients given by

$$C_\ell = \frac{1}{2\ell+1} \sum_{m=-\ell}^{\ell} |a_{\ell m}|^2 \; . \quad (9)$$

The multipole ℓ corresponds to the angular scale

$$\theta \simeq 180/\ell \text{ degrees} \; . \quad (10)$$

We have projected each sky patch onto a null signal sphere and computed the power spectrum using of the HEALPix tools (Górski et al. 1998). The coefficients were renormalized by simply dividing by the fractional coverage of the sky.

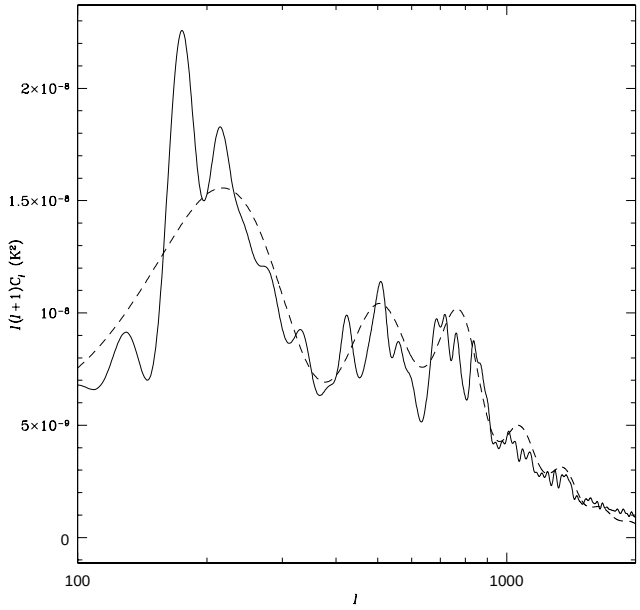

Fig. 5. CDM theoretical spectrum (dashed line) compared with the reconstructed one (solid line).

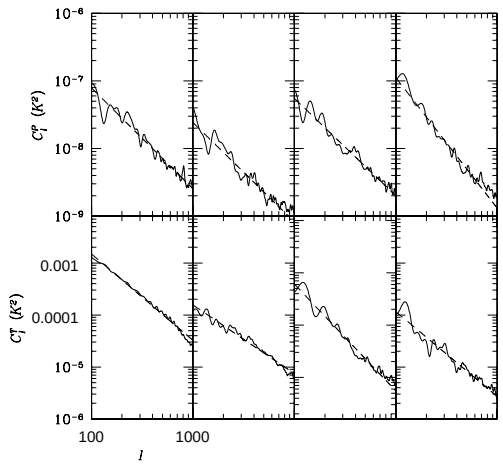

Fig. 6. Polarization (upper panels) and total intensity (lower panels) angular power spectra for the D97 region $360^\circ \geq l \geq 320^\circ$. The dashed lines represent power law fits

Note that the use of spherical harmonics is not strictly necessary, given that we are dealing with limited areas of the sky. In fact, for the common data sets, our results agree with those by Tucci et al. (2000) who resorted to a standard Fourier analysis technique.

We have tested our method using a simulation of a pure cosmological signals. We have generated an all sky map of CMB polarization as predicted by a a standard CDM model, at a resolution of about $3.5'$. We have then applied our algorithm to a randomly chosen $10^\circ \times 10^\circ$ patch. In Fig. 5 we show the recovered power spectrum for the patch compared with the theoretical one (which is, of course, an all sky average). In spite of the large oscillations, due to the sample variance, becoming larger as the angular scale approaches the patch size, the positions of the peaks are recovered.

Linear polarization is described by the Stokes parameters Q and U, from which two frame-independent quantities that can be derived: the total polarization intensity $P = \sqrt{Q^2 + U^2}$ and the polarization angle $\phi_P = \arctan(U/Q)$. P is a scalar quantity that can be expanded into spherical harmonics [eq. (8)]; its power spectrum coefficients C_ℓ^P can be computed as in eq. (9).

In order to derive the true power spectrum coefficients from the measured ones, $C_\ell^{\rm map}$, we must allow for the contribution of instrumental noise and for the effect of the detector response function $b(\ell)$:

$$C_\ell = \frac{C_\ell^{\rm map} - C_\ell^{\rm noise}}{W(\ell)} \ , \quad W(\ell) = b(\ell)^2 \ . \tag{11}$$

The beam response for each multipole is modelled by

$$b(\ell) = \exp[-\ell(\ell+1)\sigma_{\rm beam}^2/2] \ . \tag{12}$$

where $\sigma_{\rm beam} = {\rm FWHM}/(2\sqrt{2\ln 2})$ and FWHM is the full width at half maximum, in radians. In the case of D97, the beam is slightly elliptical and eq. (12) has been modified accordingly.

The instrumental noise has an approximately flat power spectrum:

$$C_\ell^{\rm noise} = 4\pi \frac{\sigma_{\rm noise}^2}{N_{\rm pixels}} \ . \tag{13}$$

For the surveys of D97, D99 and U99 we have adopted the values of the instrumental noise given by the authors (taking into account the different sensitivities reached by D97 in different regions). In the case of the BS76 data, we found convenient to treat the noise as a parameter to be determined (see subsection 4.2).

We have analyzed $10^\circ \times 10^\circ$ patches of the surveys by D97, D99 and U99. Correspondingly, the minimum value of ℓ for which the power spectrum can be estimated is $\simeq 100$, corresponding to an angular scale of about 2°: as the angular scale approaches the size of the patch, the effects of poor sampling become unacceptably large. Information on larger angular scales is provided by the BS76 data. The maximum value of ℓ is determined by the angular resolution of the survey; we have $\ell_{\rm max} \simeq 800$.

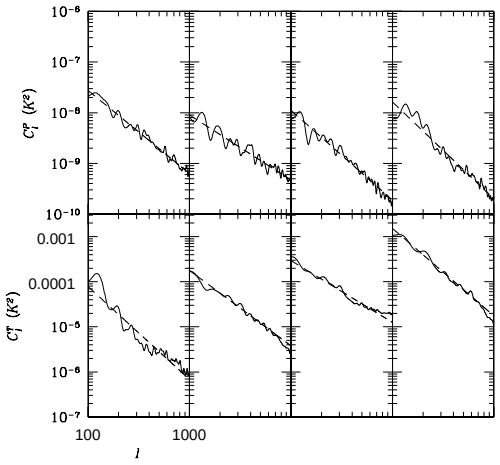

Fig. 7. Polarization (upper panels) and total intensity (lower panels) angular power spectra for the D97 region $320^\circ \geq l \geq 280^\circ$. The dashed lines represent power law fits.

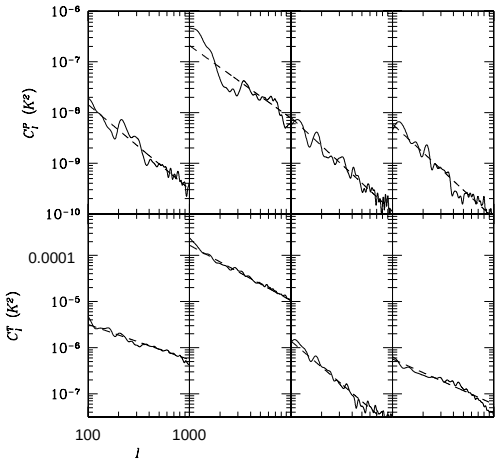

Fig. 8. Polarization (upper panels) and total intensity (lower panels) angular power spectra for the D97 region $280^\circ \geq l \geq 240^\circ$. The dashed lines represent power law fits.

4.1. Low and medium Galactic latitudes

We have focused our analysis on the low RM regions of the D97, D99, and U99 surveys. As detailed in the following, we find that these regions do possess remarkably similar polarization power spectra.

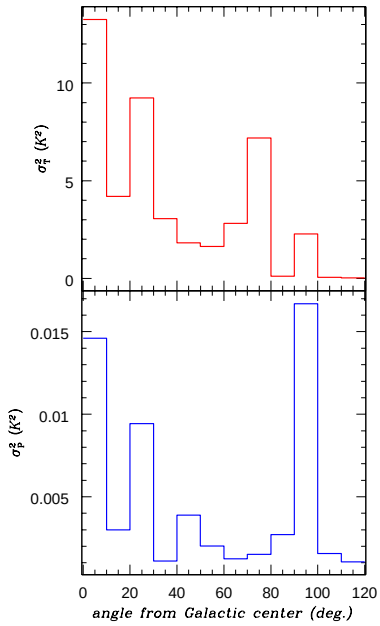

Fig. 9. Total (upper panel) and polarized intensity fluctuations in the area surveyed by D97.

Following Maino et al. (1999) we divided the D97 data in twelve $10^\circ \times 10^\circ$ subpatches, and we evaluated the power spectrum of both total intensity and polarization for each patch, over the range $100 \leq \ell \leq 800$. The results are plotted in Figs. 6–8. In each panel, the dotted line shows a power law fit ($C_\ell = \alpha \cdot \ell^\beta$).

Fig. 9 shows the variance around the mean both of total and of polarized intensities for the D97 survey, as a function of the angular distance from the galactic center, for regions 10° wide in longitude. It may be noted that polarization and total intensity fluctuations are correlated only near the Galactic center. The intensity peaks are associated to the most prominent Galactic sources, i.e. the Galactic center, the Cygnus nebulae ($280^\circ \leq l \leq 320^\circ$), and the Vela Supernova remnant ($260^\circ \leq l \leq 270^\circ$). For polarization, the signals at $320^\circ \leq l \leq 360^\circ$ are due to features appearing near the Galactic center such as the polarization "plume" (Duncan et al. 1998), while away from the Galactic center, at $l \leq 320^\circ$, only the supernova remnant produces peaks both in total and in polarized intensity.

Also, and most important, this figure shows that the total intensity fluctuations are higher by 2 or 3 orders of magnitude than the polarization ones, implying a polarization degree much lower than expected for synchrotron emission.

In fact, most of the observed intensity close to the Galactic plane appears to come from bright HII regions. For example, the region between $l = 300^\circ$ and $l = 320^\circ$

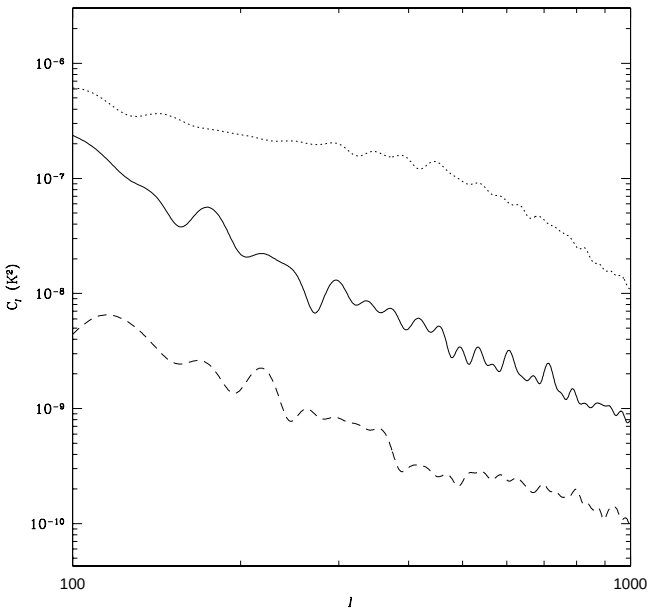

Fig. 10. Power spectrum for total intensity (dotted line) and polarization (dashed line) in the $240^\circ \leq l \leq 250^\circ$ D97 region. The solid line shows the power spectrum of total intensity after removing the most prominent sources as described in the text.

contains 95 catalogued bright HII regions (Paladini et al. 2000); the brightest ones are listed in Table 2 with their flux at 2.7 GHz and their angular sizes which are typically in the range $2' - -10'$. It is easily checked that these sources account for most, if not all, of the total intensity reported by D97. The intensity fluctuations due to them can be roughly estimated to be:

$$\sigma^2_{HII} \simeq \frac{\sum_i F_i^2}{N_{\rm pixels}} \ , \qquad (14)$$

where F_i is the flux of the $i-th$ HII region in the catalogue, scaled to the D97 resolution and to 2.4 GHz by assuming a spectral index of about -0.1, appropriate for the free-free emission. This yields $\sigma_{HII} \simeq 1$ Jy/beam, close to the value of 1.4 Jy/beam that we obtain from the D97 data.

The free-free radiation emitted by HII regions at radio wavelengths is expected to be *on average* not polarized due to the approximate spherical symmetry of the emitting region. This is the case, for instance, for the Strömgren spheres where the O or B star lies at the center of a set of concentric spheres of ionized matter. Alternative models (e.g.: the "blister" model, originally developed for the Orion Nebula by Zucherman, 1973) suggest a non-spherical symmetry and therefore the possibility of some degree of polarization. For example, polarization (*but* at optical wavelengths) has been observed for S 156 (King & Scarrot 1983), and interpreted by means of the "blister" model.

Table 2. Bright HII regions between $l = 300^\circ$ and $l = 320^\circ$.

l (deg.)	b (deg.)	$S_{2.7\rm GHz}$ (Jy)	Size ($'$)
305.1	0.1	16.3	5
305.2	0.0	62.2	7
305.2	0.2	50.1	4.8
305.4	0.2	62.2	3.5
305.6	0.0	37.6	8
307.6	-0.3	12.2	4.2
308.6	0.6	17.8	7.8
308.7	0.1	12.0	–
308.7	0.6	21.0	–
309.6	1.7	51.0	7.5
310.8	-0.4	16.6	10.9
311.9	0.1	12.9	4
311.9	0.2	11.5	4
312.3	-0.3	10.0	–
316.3	0.0	12.0	–
316.8	-0.1	43.2	2.7
317.0	0.3	15.0	7
318.0	-0.8	11.0	10.8
319.2	-0.4	12.4	5.9
320.2	0.8	11.0	1.8
320.3	-1.4	12.0	–
320.3	-1.0	23.0	–
320.4	-1.1	17.5	6
320.4	-1.0	13.0	5.6

Table 3. Power spectrum parameters of total intensity for the D97 survey. The first column is the patch center in l.

l (deg.)	α (K^2)	β	$\sigma_{\rm fit}$ (K^2)	$\sigma_{\rm signal}$ (K^2)
355	3.11	-1.66	$3.21{\cdot}10^{-5}$	$3.58{\cdot}10^{-4}$
345	$6.81{\cdot}10^{-2}$	-1.32	$7.39{\cdot}10^{-6}$	$4.47{\cdot}10^{-5}$
335	7.31	-2.04	$4.56{\cdot}10^{-5}$	$1.54{\cdot}10^{-4}$
325	$2.11{\cdot}10^{-1}$	-1.63	$1.56{\cdot}10^{-5}$	$3.89{\cdot}10^{-5}$
315	1.03	-2.06	$1.82{\cdot}10^{-5}$	$3.29{\cdot}10^{-5}$
305	$3.89{\cdot}10^{-1}$	-1.67	$5.88{\cdot}10^{-6}$	$4.19{\cdot}10^{-5}$
295	$1.62{\cdot}10^{-1}$	-1.37	$1.30{\cdot}10^{-5}$	$9.09{\cdot}10^{-5}$
285	11.6	-1.94	$5.05{\cdot}10^{-5}$	$3.31{\cdot}10^{-4}$
275	$1.08{\cdot}10^{-4}$	$-7.65{\cdot}10^{-1}$	$1.75{\cdot}10^{-7}$	$1.39{\cdot}10^{-6}$
265	$4.18{\cdot}10^{-2}$	-1.20	$8.47{\cdot}10^{-6}$	$5.64{\cdot}10^{-5}$
255	$7.64{\cdot}10^{-3}$	-1.87	$6.12{\cdot}10^{-8}$	$3.67 \cdot 10^{-7}$
245	$5.30{\cdot}10^{-5}$	$-9.84{\cdot}10^{-1}$	$2.62{\cdot}10^{-8}$	$2.01{\cdot}10^{-7}$

Another indication that sources contributing most of the intensity in the area surveyed by D97 are unpolarized is obtained by removing the highest intensity peaks and replacing their signal with the median value in an annulus around them. As shown by Fig. 10, this has the effect of strongly decreasing the amplitude of the total intensity power spectrum, particularly at intermediate and small angular scales, making its shape quite similar to that of the polarization power spectrum. Also, the polarization degree becomes $\simeq 0.3$, consistent with moderately depolarized synchrotron emission.

Table 4. Power spectrum parameters of polarized intensity for the D97 survey. The first column is the patch center in l.

l (deg.)	α (K^2)	β	$\sigma_{\rm fit}$ (K^2)	$\sigma_{\rm signal}$ (K^2)
355	$7.52\cdot10^{-5}$	-1.49	$5.37\cdot10^{-9}$	$2.13\cdot10^{-8}$
345	$2.11\cdot10^{-5}$	-1.47	$2.05\cdot10^{-9}$	$7.51\cdot10^{-9}$
335	$4.19\cdot10^{-5}$	-1.44	$4.20\cdot10^{-9}$	$1.65\cdot10^{-8}$
325	$8.10\cdot10^{-4}$	-1.93	$7.59\cdot10^{-9}$	$3.31\cdot10^{-8}$
315	$5.23\cdot10^{-5}$	-1.64	$1.16\cdot10^{-9}$	$7.25\cdot10^{-9}$
305	$3.26\cdot10^{-6}$	-1.28	$7.72\cdot10^{-10}$	$2.93\cdot10^{-9}$
295	$3.85\cdot10^{-5}$	-1.77	$6.89\cdot10^{-10}$	$2.62\cdot10^{-9}$
285	$1.08\cdot10^{-4}$	-1.91	$1.61\cdot10^{-9}$	$4.10\cdot10^{-9}$
275	$3.13\cdot10^{-5}$	-1.67	$1.00\cdot10^{-9}$	$3.97\cdot10^{-9}$
265	$1.51\cdot10^{-4}$	-1.43	$5.76\cdot10^{-8}$	$1.045\cdot10^{-7}$
250	$3.99\cdot10^{-5}$	-1.85	$4.42\cdot10^{-10}$	$1.87\cdot10^{-9}$
245	$3.11\cdot10^{-5}$	-1.86	$4.16\cdot10^{-10}$	$1.61\cdot10^{-9}$

As already mentioned, the power spectra obtained for each patch have been fitted with simple power laws:

$$C_\ell = \alpha \ell^\beta \qquad 100 \leq \ell \leq 800 \ . \tag{15}$$

The values of the parameters α and β have been obtained by minimizing the quantity:

$$\sigma^2_{\rm fit} = \frac{1}{\ell_{\rm max} - \ell_{\rm min}} \sum_{\ell=\ell_{\rm min}}^{\ell=\ell_{\rm max}} [C_\ell - \alpha \cdot \ell^\beta]^2 \ , \tag{16}$$

The best-fit values of the parameters are listed in tables 3 (for total intensity) and 4 for polarization. The tables also give the minimum $\sigma^2_{\rm fit}$ and

$$\sigma^2_{\rm signal} = \frac{1}{\ell_{\rm max} - \ell_{\rm min}} \sum_{\ell=\ell_{\rm min}}^{\ell=\ell_{\rm max}} C^2_\ell \ . \tag{17}$$

The visual impression that the fit is generally very good is quantitatively confirmed by the fact that in all cases $\sigma_{\rm fit} \ll \sigma_{\rm signal}$.

In the case of total intensity, the slope β show large variations (from $\simeq -0.5$ to $\simeq -2$) along the Galactic plane. Steeper slopes correspond to regions where diffuse emission dominates; point sources add power on small scales (large ℓ).

The situation is quite different for polarization. In general, the variations of β are substantially smaller. Also, there are several regions (at $l \leq 320°$, with exception of the Vela supernova remnant) where the power spectra are remarkably similar and described, for $100 \leq l \leq 800$, by:

$$C_\ell \ = \ (1.1 \pm 0.7) \cdot 10^{-9} \cdot \left(\frac{\ell}{450} \right)^{-1.7 \pm 0.2} \cdot$$
$$\cdot \ \left(\frac{\nu}{2.4{\rm GHz}} \right)^{-5.8} \ {\rm K}^2 \ , \tag{18}$$

where we have explicitly indicated the typical frequency dependence of Galactic synchrotron emission. We find essentially the same power spectra also for several D99 regions and for the U99 regions with low depolarization (see below). Therefore, we consider it as typical of the diffuse Galactic polarized synchrotron emission.

Table 5. Angular behavior parameters of total intensity in the 2.7GHz D99 data. The first column is the patch center in l.

l (deg.)	α (K^2)	β	$\sigma_{\rm fit}$ (K^2)	$\sigma_{\rm signal}$ (K^2)
25	$6.21\cdot10^{-1}$	-1.92	$9.63\cdot10^{-6}$	$2.86\cdot10^{-5}$
35	1.32	-1.90	$4.74\cdot10^{-6}$	$4.97\cdot10^{-5}$
45	$3.70\cdot10^{-1}$	-1.58	$1.10\cdot10^{-5}$	$6.80\cdot10^{-5}$
55	$6.70\cdot10^{-2}$	-1.97	$4.09\cdot10^{-7}$	$1.50\cdot10^{-6}$
60	$1.30\cdot10^{-3}$	-1.54	$7.56\cdot10^{-8}$	$3.09\cdot10^{-7}$

Table 6. Angular behavior parameters of polarization intensity in the 2.7 GHz D99 data. The first column is the patch center in l.

l (deg.)	α (K^2)	β	$\sigma_{\rm fit}$ (K^2)	$\sigma_{\rm signal}$ (K^2)
25	$1.64\cdot10^{-4}$	-1.79	$2.70\cdot10^{-9}$	$1.17\cdot10^{-8}$
35	$1.25\cdot10^{-4}$	-1.72	$4.00\cdot10^{-9}$	$1.04\cdot10^{-8}$
45	$3.97\cdot10^{-5}$	-1.55	$1.66\cdot10^{-9}$	$8.71\cdot10^{-9}$
55	$1.30\cdot10^{-4}$	-1.98	$9.93\cdot10^{-10}$	$2.88\cdot10^{-9}$
60	$6.46\cdot10^{-5}$	-1.93	$8.20\cdot10^{-10}$	$1.93\cdot10^{-9}$

The D99 database at 2.7GHz is on the Galactic plane at $-5° \leq b \leq 5°$, $4.9° \leq l \leq 74°$. We selected five squared $10° \times 10°$ patches centered in $l = 25°, 35°, 45°, 55°, 60°$. The angular power spectra are reported in Figure 11, and the values for the fit with exponential power law are in tables 5,6. The dotted lines plotted in the polarization spectra represent the the fit in eq.(18). The spectra are completely consistent with what we obtain in D97, once we have rescaled the signals at the same frequency using a typical synchrotron spectral index -2.9: the total intensity signal is noticeably dominant with respect to the polarization one, and again, as we go away from the Galactic center, at $l \geq 50°$, we find a polarization signal consistent with eq.(18).

Let us consider now the three patches from the U99 data at 1.4 GHz, which are consistent with low depolarization, with centers and side given by:

$$1 \ : \ l = 50° \ , b = 12°, \ \Delta l = \ 10°, \ \Delta b = 15°,$$
$$2 \ : \ l = 146.4° \ , b = 6.8°, \ \Delta l = 12° \ , \ \Delta b = 6.3° \ . \tag{19}$$
$$3 \ : \ l = 196.8° \ , b = 11.2°, \ \Delta l = \Delta b = \ 6.7° \ . \tag{20}$$

In Fig. 12 we plot the angular power spectra of these regions, for polarized (top) and total intensity (bottom): as in the previous figures, the dashed line is the fit of the spectra with power laws reported in table 7. We reported also the dotted line representing eq.(18), rescaled at the U99 of 1.4 GHz by using simply a synchrotron power law index -2.9. As it is evident there is a good agreement between the two surveys, indicating that the same synchrotron background polarized radiation extends up to latitude $b \simeq 10°$ maintaining unaltered its properties. We can therefore improve our measure eq.(18) of the Galactic synchrotron power spectrum from diffuse polarized emission by con-

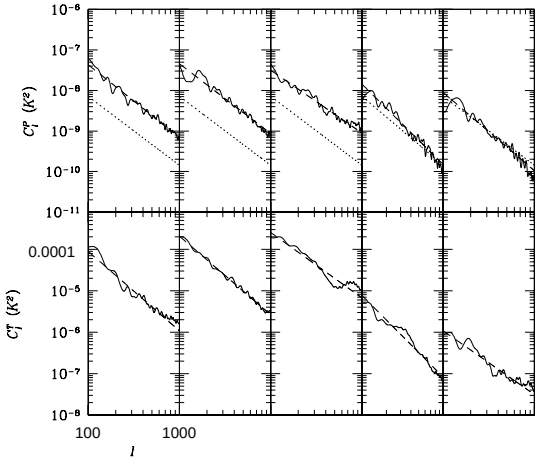

Fig. 11. Polarization intensity (top) and total intensity (bottom) angular power spectra for $20^\circ \geq l \geq 65^\circ$ in the D99 database at 2.7GHz. The dashed lines represent power law fits. The dotted line represent the power spectrum from D97, rescaled at 2.7GHz.

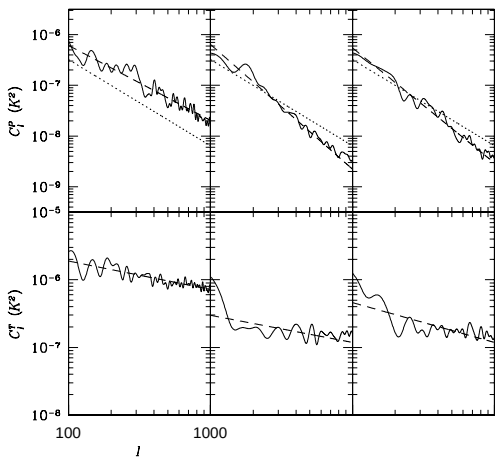

Fig. 12. Polarization intensity (top) and total intensity (bottom) angular power spectra for the three low depolarization areas in the U99 database at 1.4GHz. The dashed lines represent power law fits. The dotted line represent the power spectrum from D97, rescaled at 1.4GHz.

Table 7. Angular behavior parameters of polarization (PI) and total intensity (I) in the U99 data at 1.4 GHz.

region	α (K^2)	β	$\sigma_{\rm fit}$ (K^2)	$\sigma_{\rm signal}$ (K^2)
1 (PI)	$5.61{\cdot}10^{-4}$	-1.48	$4.81{\cdot}10^{-8}$	$1.68{\cdot}10^{-7}$
2 (PI)	$5.34{\cdot}10^{-2}$	-2.46	$3.61{\cdot}10^{-8}$	$1.09{\cdot}10^{-7}$
3 (PI)	$1.90{\cdot}10^{-2}$	-2.27	$1.49{\cdot}10^{-8}$	$1.05{\cdot}10^{-7}$
1 (I)	$1.31{\cdot}10^{-5}$	$-4.20{\cdot}10^{-1}$	$2.14{\cdot}10^{-7}$	$1.17{\cdot}10^{-6}$
2 (I)	$1.89{\cdot}10^{-6}$	$-4.01{\cdot}10^{-1}$	$1.06{\cdot}10^{-7}$	$2.25{\cdot}10^{-7}$
3 (I)	$6.92{\cdot}10^{-6}$	$-5.89{\cdot}10^{-1}$	$1.14{\cdot}10^{-7}$	$2.84{\cdot}10^{-7}$

sidering the regions from U99 and D99 at $l \geq 50^\circ$. The result, once all the data have been rescaled at 2.4 GHz, is

$$C_\ell \;=\; (1.2 \pm 0.8) \cdot 10^{-9} \cdot \left(\frac{\ell}{450}\right)^{-1.8\pm0.3} \cdot \\ \cdot \;\left(\frac{\nu}{2.4{\rm GHz}}\right)^{-5.8} \;{\rm K}^2 \;, \qquad (21)$$

which substantially confirms our previous result obtained from D97.

4.2. High galactic latitudes

The accurate and high resolution D97, D99 and U99 polarization surveys allow to understand the correlation properties of polarized synchrotron emission at multipoles larger than ~ 100, owing to the limited extent of the patches we can extract from the observed regions, and cover regions at low or intermediate galactic latitudes.

In order to extend the analysis of the polarized synchrotron fluctuation power spectrum at superdegree angular scales and at high galactic latitude we have exploited the BS76 polarization measurements, the only data currently available that cover about half of the sky.

We restrict the present analysis to the 1.411 GHz channel, for a simpler comparison with the high resolution surveys. As we already mentioned in the Introduction, at 1.411 GHz the BS76 measures refer to 1726 positions covering approximately half sky at $l \gtrsim 0^\circ$ with a FWHM resolution of about 0.6°. However, the sky is significantly undersampled, particularly when the whole observed region is considered. We project the original data into HEALPix maps at different resolutions $\theta \simeq 3600/n_{side}$ arcminutes, where n_{side} is the HEALPix resolution parameter (Górski et al. 1998). The whole sky map is essentially filled only at low resolutions, $\theta \simeq 7.3^\circ$ or 3.6°, corresponding to $n_{side} = 8$ or 16 respectively, that allow to estimate the angular power spectrum only at $\ell \lesssim 50$. On the other hand, we can take advantage from some regions where the sky is better sampled and/or interpolate the existing data to fill maps at higher resolutions, $\theta \simeq 1.8^\circ \div 0.9^\circ$, corresponding to $n_{side} = 32$ or 64 respectively, to try an approximate estimate of the power spectrum at higher multipoles, up to $\ell \simeq 100 \div 200$, and reach the multipole range where the power spectrum estimation from high resolution surveys does not suffer of significant boundary effects introduced by patch sizes. It is important in any case to fill the map

through interpolations to avoid the "holes" corresponding to unobserved pixels. In fact, they artificially alter the power spectrum estimation by introducing spurious (flat) power at the pixel scale, being seen like "negative sources" in the power spectrum estimation (see La Porta & Burigana 2000 for further details). We do not expect crucial artifacts by this treatment, since the analysis of the polarized synchrotron fluctuations at angular smaller scales presented above indicates that the power significantly decreases toward high multipoles. Of course, by comparing the power spectrum derived by analyzing the whole map and some regions where the sky is better sampled (and, consequently, the possible interpolation effects less relevant) we can test the effect of these approximations.

We identified three relatively highly sampled regions in the maps derived from the BS76 data: 1) a patch at low galactic latitude ($110^\circ \leq l \leq 160^\circ$, $0^\circ \leq b \leq 20^\circ$), that can be used for a comparison with the above results at higher resolutions and to extend the analysis of the galactic plane regions to low multipoles; 2) a relative wide patch at the North pole [($5^\circ \leq l \leq 80^\circ$, $b \geq 50^\circ$) together with ($0^\circ \leq l \leq 5^\circ$, $b \geq 60^\circ$) and ($335^\circ \leq l \leq 360^\circ$, $b \geq 60^\circ$)]; 3) a relative small but better sampled patch at the North pole, ($10^\circ \leq l \leq 80^\circ$, $b \geq 70^\circ$), included in the above patch. The analysis of the patches 2) and 3) allows to extend the polarized synchrotron power spectrum estimation at high galactic latitudes, that are crucial for the evaluation of foreground contamination in the recovery of the CMB polarization power spectrum; in addition, the comparison between the power spectra derived from these patches provide indications to understand the effects introduced by the adopted interpolation techniques and the limited patch sizes, although intrinsic physical differences are certainly present.

The results, scaled to the case of a full sky coverage, are shown in Fig. 13, for $30 \lesssim \ell \lesssim 200$; at multipoles $\lesssim 30$ boundary effects are relevant particularly for the patches. At multipoles $\ell \approx 100$ one can note a flattening of the power spectrum with respect to the steep shape at lower multipoles, particularly in the case of the spectrum derived from the whole map. At $\ell \approx 100$ the power of the instrumental noise clearly emerges.

We fit the C_ℓ so derived as a sum of a power law, representing the polarized synchrotron power spectrum, plus a constant level, accounting for the instrumental noise power; we use the MINUITS tools of the CERN libraries (available at the WEB site `http://cern.web.cern.ch/CERN/`) and find that it is more advantageous for the fit stability and accuracy to work by using the variables $\log \ell$ and $\log C_\ell$. We avoid here to take into account the beam smoothing, being its effect important at multipoles higher than those at which the noise power becomes significantly larger than the polarized synchrotron power. Clearly the noise power levels estimated in this way depend also on the data projection and interpolation methods; we have checked that they are approximately in agreement with the estimates based on the quoted sensitivities in the original data tabulation. The results of the MIGRAD fit for the whole map and the three patches are shown as solid lines in the four panels of Fig. 14: the upper solid lines refer to the sum of the polarized synchrotron and noise powers, the bottom solid lines to the polarized synchrotron powers alone. In the case of the patch 1) we show also (dashed lines) the alternative SIMPLEX fit result which works also quite well and suggests a power law with spectral index closer to -2 than to the value, ~ -3, characterizing the other fits.

(From MIGRAD) We find:

$$C_\ell \simeq (9.4 \cdot 10^{-1} \cdot \ell^{-3.3} + 3.2 \cdot 10^{-7})\ \mathrm{K}^2 \tag{22}$$

for the whole map,

$$C_\ell \simeq (1.5 \cdot \ell^{-3.1} + 4.8 \cdot 10^{-7})\ \mathrm{K}^2 \tag{23}$$

for the patch 2),

$$C_\ell \simeq (1.1 \cdot \ell^{-2.8} + 8.7 \cdot 10^{-7})\ \mathrm{K}^2 \tag{24}$$

for the patch 3), and

$$C_\ell \simeq (8.8 \cdot 10^{-1} \cdot \ell^{-2.85} + 1.1 \cdot 10^{-6})\ \mathrm{K}^2 \tag{25}$$

for the patch 1); in this case another possible (SIMPLEX) reasonable fit is

$$C_\ell \simeq (2.0 \cdot 10^{-2} \cdot \ell^{-1.9} + 2.2 \cdot 10^{-7})\ \mathrm{K}^2\,. \tag{26}$$

The three patches considered here show power spectra in agreement one each other within a factor of about 2; for instance, by considering eqs.(23-25) and taking $\ell = 50$ as reference multipole, and scaling again at 2.4 GHz, for the synchrotron contribution we have

$$C_\ell \ = \ (4 \pm 3) \cdot 10^{-7} \cdot \left(\frac{\ell}{50}\right)^{-2.9 \pm 0.2} \cdot \\ \cdot \ \left(\frac{\nu}{2.4 GHz}\right)^{-5.8}\ \mathrm{K}^2\,. \tag{27}$$

No significant differences are found for the polarized synchrotron power spectrum between the considered region on the galactic plane and the North polar region. The power spectrum found for the whole map exhibits a slope quite close to that of the three considered patches and a level about 3–6 times smaller, due to the relative lower level of polarization intensity and fluctuations in the regions far from the patches considered here.

In spite of their poor sky sampling and of all the approximations introduced to treat them, it is remarkable that the BS76 data indicate both a power level at multipoles about 100 in quite good agreement with the results derived from more recent surveys with a slightly larger slope. This suggests that, at least on superdegree angular scales, the fluctuations of the diffuse Galactic polarized synchrotron emission does not decrease going to high latitudes.

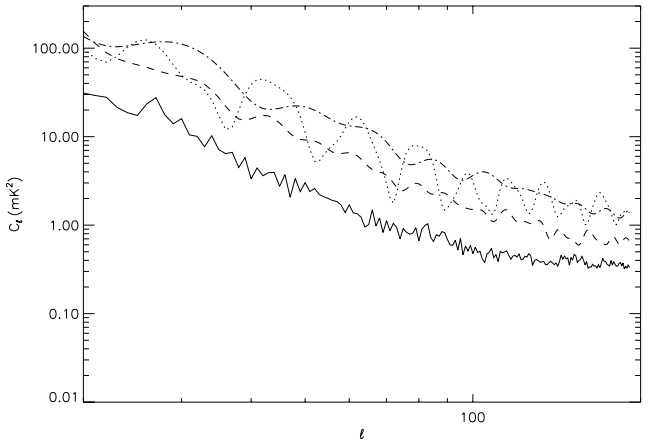

Fig. 13. Angular power spectrum of polarized synchrotron emission at 1.411 GHz at low multipoles as derived by projecting into a map the Brouw & Spoelstra (1976) data for different sky regions: the whole map (solid line), the region 1) (dotted line), the region 2) (dashed line) and the region 3) (dotted-dashed line).

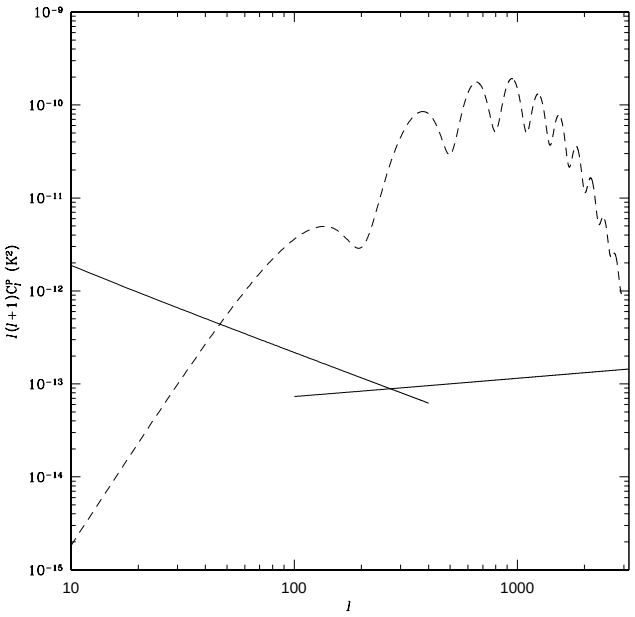

Fig. 15. Comparison of CMB expected polarized signal (dashed line) with Galactic synchrotron diffuse polarized emission at 100 GHz (solid lines).

In any case, the signals found in our analysis are unlikely to represent a problem for future MAP and Planck measurement. We extrapolate our results at microwave frequencies to estimate the level of contamination to the CMB radiation from the foreground emission investigated here. In Figure 15 we plot the expected level of polarization fluctuation for a CDM model as the one in Fig. 5 together with the two expected level of contamination from eq.21 and eq.(27) extrapolated at 100 GHz. It can be noted how the CMB is expected to be largely dominant with respect to this kind of polarized foreground, starting from $\ell \simeq 50$ up to the highest multipoles which are experimentally achievable by MAP and Planck.

5. Conclusions

We have analyzed the existing database for diffuse Galactic polarized emission at GHz frequencies. The data come from the most recent surveys with few arcminutes resolution at low and medium Galactic latitudes (Duncan et al. 1997, 1999, Uyaniker et al. 1999), as well as from higher latitudes including the north Galactic pole at the degree resolution (Brouw & Spoelstra 1976).

Our analysis shows that it is unlikely to be a serious limitation to measurements of CMB polarization fluctuations at the highest frequencies of the MAP and Planck/LFI instruments, at least for $\ell \geq 50$, and even at relatively low Galactic latitudes. This is very encouraging since the highest sensitivity polarization maps that will be produced by the Planck satellite will cover regions around the Ecliptic poles, which are at moderate Galactic latitudes ($|b| \simeq 27^\circ$).

This conclusion is substantiated by a careful analysis of depolarization effects. Regions were identified where rotation measures of pulsars and extragalactic sources, the high polarization degree and, in some cases, data on the distribution of polarization vectors and on the Galactic magnetic field, consistently indicate that depolarization must be small.

The low polarization degree of radio emission close to the Galactic plane, found also in low-depolarization regions, is interpreted as due to large contributions to the observed intensity from unpolarized sources, primarily strong HII regions. Since such sources are concentrated on the Galactic plane, estimates of the power spectrum of total intensity at low Galactic latitudes are not representative of the spatial distribution of Galactic emission far from the plane.

The extrapolation of our results to different regions of the Galaxy, and in particular to higher Galactic latitudes is obviously not straightforward. In general, we expect that the power spectrum of total and polarized emission varies across the sky. For example, it is reasonable to expect less small scale structure in the general anticenter region because emission cells have generally larger angular sizes because they are, on average, relatively closer.

In general, it is likely that the amplitude of the power spectrum of Galactic emission decreases with increasing Galactic latitude as a consequence of the decreased emission. Also, as pointed out by Davies & Wilkinson (1999), the magnetic field pattern may be more ordered at high Galactic latitudes, resulting in less small scale structure. Moreover, narrow depolarizing structures, that may be present in regions where depolarization is generally small,

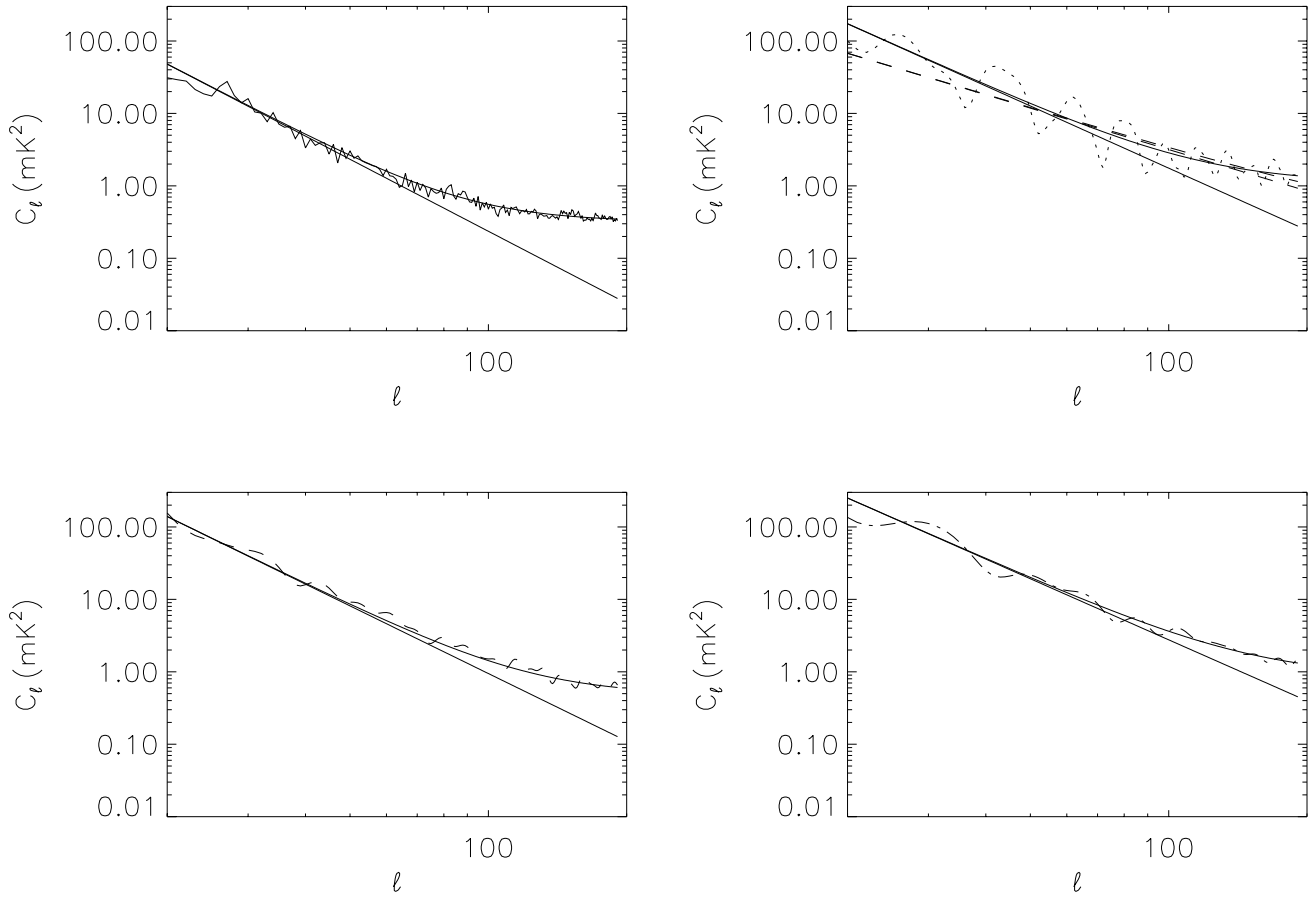

Fig. 14. Fit to the angular power spectra of polarized synchrotron emission at 1.411 GHz of Fig. 1. Top left panel: whole map; top right panel: patch 1); bottom left panel: patch 2); bottom right panel: patch 3). Note the oscillations at low l somewhat larger in the case of the patch 3) than in the case of the patch 2) – which contains the patch 3) – principally due to the smaller extent of patch 3). See the text for further details.

may again increasing the amplitude of the the polarization fluctuations on small scales. Unfortunately, we can not have a check of this issue since we have only superdegree data covering all latitudes. However, our results indicate that on subdegree angular scales no evidence of such a decrease is seen by comparing data from low and medium Galactic latitudes up to $b \simeq 20^\circ$ (from Duncan et al. 1997, 1999 and Uyaniker et al. 1999, respectively). On higher Galactic latitudes the data from Brouw & Spoelstra (1976) suggest that, at least on superdegree angular scales, emission do not decrease even at the Galactic poles.

In any case, it seems very likely that the power spectrum of polarized Galactic emission on subdegree angular scales and well above the Galactic plane has a smaller or at most equal amplitude than is found in the low-depolarization regions analyzed here. Our conclusion that polarized synchrotron emission will not hamper CMB polarization measurements thus appears to be robust. We found, in antenna temperature, the following measure: for $100 \leq \ell \leq 800$ and $b \leq 20^\circ$ we find

$$C_\ell \;=\; (1.2 \pm 0.8) \cdot 10^{-9} \cdot \left(\frac{\ell}{450}\right)^{-1.7 \pm 0.3} \cdot \\ \cdot \;\left(\frac{\nu}{2.4\mathrm{GHz}}\right)^{-5.8}\; K^2\,, \qquad (28)$$

while for $\ell \leq 100$ and all latitudes we find

$$C_\ell \;=\; 4 \pm 3 \cdot 10^{-7} \cdot \left(\frac{\ell}{50}\right)^{-2.9 \pm 0.2} \cdot \\ \cdot \;\left(\frac{\nu}{2.4\mathrm{GHz}}\right)^{-5.8}\; \mathrm{K}^2\,. \qquad (29)$$

Finally, the distributions of both total and polarized Galactic emissions was shown to be non-Gaussian at a high significance level. This may be a problem for methods of component separation using Wiener filtering, which assumes Gaussian distributions. On the other hand, it allows the application of Independent Component Analysis techniques (Baccigalupi et al. 2000) which just rely on the

assumption that all but at most one of the components to be separated have a non-Gaussian distribution.

Acknowledgements. Thanks are due to A.R. Duncan and to B. Uyaniker who have generously made available their maps through the Web and also provided additional information on their results. We are grateful to T.A.T. Spoelstra for his kind clearifications. This work was supported in part by ASI and MURST.

References

Baccigalupi C., Bedini L., Burigana C., De Zotti G., Farusi A., Maino D., Maris M., Perrotta F., Salerno E., Toffolatti L., Tonazzini A., 2000, MNRAS in press, astro-ph/0005543

Bingham R.G. & Shakeshaft J.R. 1967, MNRAS 136, 347

Bouchet F.R., Prunet S., Sethi S.K., 1999, MNRAS 302, 663

Brouw W.N., Spoelstra T.A.T., 1976, A&AS 26, 129 (BS76)

Broten, N.W., MacLeod J.M., Vallee J.P., 1988, Ap.& SS.141, 303

Burn B.J., 1966, MNRAS 133, 67

Clegg A.W., Cordes J.M., Simonetti J.M., Kulkarni S.R., 1992Ap.J. 386, 143

Davies R.D., Wilkinson A., 1999, In: de Oliveira-Costa A., Tegmark M. (eds.) Microwave Foregrounds, ASP Conf. Ser. Vol. 181, ASP, San Francisco, p. 77

De Zotti G., Gruppioni C., Ciliegi P., Burigana C., Danese L., 1999, NA 4, 481

Franceschini A., Toffolatti L., Danese L., de Zotti G., 1989, Ap.J. 344, 35

Draine B.T., Lazarian A., 1999, In: de Oliveira-Costa A., Tegmark M. (eds.) Microwave Foregrounds, ASP Conf. Ser. Vol. 181, ASP, San Francisco, p. 133

Duncan A.R., Haynes R.F., Jones K.L., Stewart R.T., 1997, MNRAS 291, 279 (D97)

Duncan A.R., Haynes R.F., Reich W., Reich P. & Gray A.D. 1998, MNRAS 291, 279

Duncan A.R., Reich P., Reich W., Fürst E., 1999, A&A 350, 447 (D99)

Duncan A.R., Stewart R.T., Haynes R.F., Jones K.L., 1995, MNRAS 277, 36

Gardner F.F., Whiteoak J.B., 1966, ARA& A 4, 245

Ginzburg V.L., Syrovatskii S.I., 1965, ARA& A 3, 297

Grski K.M., Wandelt B., Hansen F., Hivon E., Stompor R., Banday A.J., Bartelmann M., 2000, packadge available at the web site `http://www.eso.org/ kgorski/healpix/`

Han J.L., Beck R., Ehle M., Haynes R.F., Wielebinski R. 1999, A& A 348, 405

Keating B., Timbie P., Polnarev A., Steinberger J., 1998, ApJ 495, 580

King D.J & Scarrot S.M, 1983, MNRAS, 202, 11

La Porta, L. & Burigana, C. (2000), Int. Rep. TeSRE/CNR, in preparation

Lazarian A., Draine B.T., 2000, ApJ 536, L15

Mandolesi N., Lawrence C.R., Bersanelli M., et al., 1998, Low Frequency Instrument for Planck. A proposal to the European Space Agency

Maino D., Baccigalupi C., Burigana C., Maris M., Perrotta F., 1999 contribution at the Planck-LFI meeting in Capri, October 1999

Manchester R.N., Johnston S., 1995, Ap.J. 441, 65

Navarro J., Manchester R.N., Sandhu J.S., Kulkarni S.R., Bailes M., 1997, Ap.J. 486, 1019

Paladini R., Bersanelli M. & Maino D., 2000, submitted to A& A

Prunet S., Sethi S.K., Bouchet F.R., Miville-Deschênes M.-A., 1998, A&A 339, 187

Puget J.-L., Efstathiou G., Lamarre J.M., et al., 1998, High Frequency Instrument for the Planck mission. A proposal to the European Space Agency

Sironi G., Boella G., Bonelli G., Gervasi M., Vaccari A., Zannoni M., 1999, proceedings of the EC-TMR Conference 3K Cosmology, edited by Maiani L., Melchiorri F., Vittorio N., Woodbury, N.Y., American Institute of Physics, vol. 476, 1999., p.149

Spoelstra T.A.T., 1984, A& A 135, 238

Taylor J.H., Manchester R.N., Lyne A.G., 1993, Ap.J.S. 88, 529

Staggs S.T., Gundersen J.O., Church S.E., 1999, In: de Oliveira-Costa A., Tegmark M. (eds.) Microwave Foregrounds, ASP Conf. Ser. Vol. 181, ASP, San Francisco, p. 299

Tucci M., Carretti E., Cecchini S., Fabbri R., Orsini M., Pierpaoli E., 2000, NA, in press

Uyaniker B., Fürst E., Reich W., Reich P., Wielebinski R., 1998, A&AS 132, 401

Uyaniker B., Fürst E., Reich W., Reich P., Wielebinski R., 1999, A&AS 138, 31 (U99)

Zaldarriaga M., 1998, ApJ 503, 1